Accepted Manuscript

Journal of the Geological Society

Marine redox dynamics and biotic response to the mid-Silurian Ireviken Extinction Event in a mid-shelf setting

Yuxuan Wang, Paul B. Wignall, Yijun Xiong, David K. Loydell, Jeffrey Peakall, Jaco H. Baas, Benjamin J.W. Mills & Simon W. Poulton

DOI: https://doi.org/10.1144/jgs2023-155

To access the most recent version of this article, please click the DOI URL in the line above. When citing this article please include the above DOI.

This article is part of the Chemical Evolution of the Mid-Paleozoic Earth System and Biotic Response collection available at: https://www.lyellcollection.org/topic/collections/chemical-evolution-of-the-mid-paleozoic-earth-system

Received 14 September 2023
Revised 5 February 2024
Accepted 13 March 2024

Supplementary material at https://doi.org/10.6084/m9.figshare.c.7165009

Marine redox dynamics and biotic response to the mid-Silurian Ireviken Extinction Event in a mid-shelf setting

Yuxuan Wang[1], Paul B. Wignall[1], Yijun Xiong[1], David K. Loydell[2], Jeffrey Peakall[1], Jaco H. Baas[3], Benjamin J.W. Mills[1], Simon W. Poulton[1]

[1]*School of Earth and Environment, University of Leeds, Leeds LS2 9JT, UK*
[2]*School of the Environment, Geography and Geosciences, University of Portsmouth, Burnaby Road, Portsmouth PO1 3QL, UK*
[3]*School of Ocean Sciences, Bangor University, Menai Bridge, Isle of Anglesey, LL59 5AB, UK*

Abstract

The early Silurian Llandovery–Wenlock boundary interval was marked by significant marine perturbations and biotic turnover, culminating in the Ireviken Extinction Event (IEE) and the Early Sheinwoodian Carbon Isotope Excursion (ESCIE). Here, we apply multiple independent redox proxies to the early Wenlock Buttington section, which was deposited in a mid-shelf location in the Welsh Basin, UK. To account for regional geochemical variability in marine sediments due to factors such as sediment provenance, we first define oxic baseline values for the Welsh basin, utilizing deeper water, well-oxygenated intervals of late Llandovery age. Our approach documents unstable, oscillating redox conditions on the mid shelf at Buttington. We suggest that these dynamic redox fluctuations are likely to relate to changes in the position of the chemocline or a migrating oxygen minimum zone. Benthic biota such as trilobites, brachiopods, bivalves and gastropods appear to have been relatively unaffected by fluctuating oxic-ferruginous conditions, but were more severely impacted by the development of euxinia, highlighting the inhibiting role of toxic sulfides. By contrast, the redox perturbations appear to have placed extreme stress on graptolites, causing many extinction losses regardless of the specific development of euxinia.

The Llandovery–Wenlock boundary of the early Silurian is marked by both marine environmental changes and biotic turnover (Calner, 2008; Lehnert et al., 2010; Loydell and Large, 2019). The Ireviken extinction event (IEE), which was a crisis interval for conodonts, chitinozoans, trilobites and brachiopods (Jeppsson, 1997; Jeppsson et al., 1998; Hints et al., 2006), straddles this boundary and coincides with the onset of a substantial positive isotope excursion in both carbonate ($\delta^{13}C_{carb}$) and organic carbon ($\delta^{13}C_{org}$), termed the early Sheinwoodian carbon isotope excursion (ESCIE; Saltzman, 2001; Munnecke et al., 2003; Cramer et al., 2012; Oborny et al., 2020; Hartke et al., 2021). The start of ESCIE can be dated to the late *murchisoni* graptolite-Biozone (Figs. 1 & 2; Kaljo and Martma, 2006; Loydell and Frýda, 2007). Values then peak around the *riccartonensis*

Biozone, before the excursion ends in the mid Sheinwoodian (Fig. 2), during the *belophorus* (formerly *flexilis*) Biozone (Loydell and Frýda, 2007). The ESCIE has been attributed to enhanced organic carbon burial in anoxic deep ocean and intra-cratonic basinal settings, at a time when there was an expansion of carbonate platforms in lower latitude epeiric seas (Jeppsson, 1990; Bickert et al., 1997; Cramer and Saltzman, 2007).

Hypoxia-triggered marine extinctions and carbon cycle perturbations appear to have been a recurring scenario during the Silurian (Jeppsson et al., 1998; Calner, 2008; Young et al., 2020), and a recent study in the Baltic region has shown that the early Sheinwoodian saw the expansion of euxinia (sulfidic water column conditions) in a continental margin location, with potential consequences for the resident biota (Young et al., 2019). Although both the IEE and ESCIE are observed globally, potential sulphur isotope (e.g., carbonate-associated sulphate ($\delta^{34}S_{CAS}$) and pyrite sulphur ($\delta^{34}S_{py}$) isotopes) evidence for widespread shelf euxinia (Rose et al., 2019; Richardson et al., 2021) has been questioned, based on a suggested dominant control of lithofacies variability on isotope compositions due to regional sea-level change (Pasquier et al., 2021). In this scenario, observed increases in S isotope compositions may have been a consequence of enhanced closed system diagenesis as local sedimentation rate varied, rather than being due to elevated water column $\delta^{34}S$ compositions through sulphate drawdown under widespread euxinic conditions. Furthermore, most studies have concentrated on shallow-water carbonate platforms (Jeppsson, 1997; Munnecke et al., 2003; Lehnert et al., 2010; Hughes and Ray, 2016; Yan et al., 2022), whilst the redox state of deeper siliciclastic successions remains more poorly constrained.

Here, we report a reconstruction of the redox history of the early Wenlock (Sheinwoodian) interval from a mid-shelf section in the Welsh Basin (Fig. 1), using a combination of Fe speciation and redox-sensitive trace metal systematics. Our focus is on high-resolution, siliciclastic samples from Buttington, east Wales (Loydell and Large, 2019). However, since baseline oxic geochemical values can vary between basins, we have also assessed samples from two deeper-water sections from

within the Welsh Basin, in order to characterize the oxic geochemical signature in the region. The Buttington section has been the subject of detailed palaeoecological investigation (Loydell and Large, 2019), and thus provides an ideal opportunity to investigate the biotic response of a mid-shelf region to the major environmental perturbations that occurred during the early Wenlock.

Study area and sampled sections

The Ordovician–Silurian Welsh Basin records deposition on the northerly-facing margin of the Avalonia microcontinent, and has the Midland Platform of central England on its eastern margin (James, 2005; Fig. 1A). The microcontinent drifted northwards as the Iapetus Ocean subducted beneath the Laurentia continent, and by the early Silurian the ocean had narrowed considerably (Stone, 2014). Our focus is on three lower Silurian mudstone-dominated sections from the basin centre (Borth section), deep outer shelf (River Banwy section) and mid shelf (Buttington section) (Fig. 1B). The Borth section (Fig. 1C) is of early Telychian (late Llandovery) age (i.e., prior to the onset of the IEE and ESCIE) and records a mudstone-dominated turbidite succession developed distal to the turbiditic sandstones of the Aberystwyth Grits (Baker and Baas, 2020). The River Banwy location comprises a continuous mudstone-dominated section spanning much of the Llandovery–lower Wenlock (Fig.1C; Loydell and Fryda, 2007). We utilize the Borth and Banwy sections to provide regional baseline oxic values for consideration of redox proxy data from the key Buttington section, since such data may be particularly basin-specific (Algeo and Li, 2020; Poulton, 2021; Li et al., 2023). Hence, for the Banwy River section, our focus is only on samples from the upper *crispus* to lower *centrifugus* graptolite biozones, prior to the onset of the IEE and ESCIE (Fig. 1C).

The Buttington section comprises early Silurian strata, including most of the Telychian Stage and the lower part of the Sheinwoodian Stage (Fig. 1C). The lower Cefn Formation comprises interbedded tempestite sandstones and mudstones (Loydell and Cave, 1993) that unconformably overlie Ordovician shales (Fig. 3). The overlying Tarannon Mudstone Formation predominantly

comprises green and purple shale. Finally, the Trewern Brook Formation is a dark grey mudstone, with an 8.75 m-thick olive calcareous silty mudstone unit at its base (Butterley Mudstone Member) and several thin bentonites (Fig. 3; Cave and Dixon, 1993; Loydell and Cave, 1993). Our focus is on the upper *murchisoni* to *riccartonensis* biozones of the Sheinwoodian Stage, which were sampled in an active quarry (Buttington) near Welshpool, in Powys, Wales. Previous research has established a detailed graptolite record and the carbon isotope chemostratigraphy for this section, demonstrating that the samples correspond to the early part of the ESCIE and the onset of the peak part of the IEE (Loydell et al., 2014; Loydell and Large, 2019).

Materials and Methods

Samples

High-resolution sampling was conducted at Buttington, with 120 samples of dark grey mudstone collected from a 12.5 m-thick section from the uppermost Butterley Mudstone Member (lower Sheinwoodian) and continuing into the lower Trewern Brook Formation (Fig. 3). From the Banwy River section, ten samples of light grey mudstones from the Telychian *crispus* to *centrifugus* biozones were analysed, whilst for the coastal cliff section at Borth (see Cave and Loydell, 1997; James, 2005), 78 pale grey mudstones from the early Telychian *guerichi* Biozone of the Borth Mudstones Formation were analysed (Fig. 1C). All samples underwent careful removal of weathered surfaces prior to analysis.

Total organic carbon

For the determination of total organic carbon (TOC), sample powders were pretreated with 10% HCl and shaken overnight twice to remove carbonate phases. The residues were then washed at least three times with Milli-Q water to eliminate residual acid. Dried and powdered samples were analyzed on a LECO CS-230 analyzer. Replicate analyses of certified standards (Soil 502–309, n=16) gave a relative standard deviation (RSD) of <3%, and measurements were within 2% of certified values.

Iron speciation

Iron speciation was determined via an operationally-defined sequential extraction scheme for unsulfidized phases (Poulton and Canfield, 2005; Poulton, 2021), and a separate extraction scheme for Fe sulfides (Canfield et al., 1986). These techniques target Fe in carbonate phases (Fe_{carb}), Fe (oxyhydr)oxides (Fe_{ox}), magnetite Fe (Fe_{mag}), and sulfide-bound Fe (Fe_{py}), which together comprise highly reactive Fe (Fe_{HR}). The Fe_{carb} pool was extracted using Na-acetate solution at pH 4.5 and 50°C for 48 h, followed by treatment with Na-dithionate for 2 h at room temperature to extract Fe_{ox}, and then extraction of the Fe_{mag} pool using an ammonium oxalate solution for 6 h at room temperature. Iron concentrations were then determined via atomic absorption spectrometry. Replicate analyses (n=8) of international reference material WHIT (Alcott et al., 2020) gave an RSD of <5% for all stages, and analyses were within 3% of certified values. Sulfide-bound Fe, including acid volatile sulfide (Fe_{AVS}; below detection in all cases) and pyrite (Fe_{py}), was extracted using a two-step hydrochloric acid (HCl) and chromous chloride ($CrCl_2$) technique (Canfield et al., 1986). The liberated H_2S was collected as Ag_2S, which was then determined gravimetrically and converted stoichiometrically to Fe_{py} concentrations, with an RSD of <5%.

Bulk element concentrations

Approximately 80 mg of powder were ashed at 550°C for 8 h, followed by dissolution with HNO_3–HF–$HClO_4$. After evaporation to dryness, the samples were treated with boric acid (H_3BO_3) and heated to dryness again, prior to being re-dissolved with hot HNO_3. Total element concentrations were then analyzed via ICP-OES (ThermoFisher iCAP 7400) for major elements and ICP-MS (ThermoFisher iCAPQc) for trace elements. Replicate extractions of international sediment standard SGR-1 yielded RSDs of <2% for all major and trace elements of interest, and analyses were within 3% of certified values.

Framework for redox interpretations

To reconstruct water column redox conditions, we utilized independent inorganic redox proxies based on Fe speciation and redox sensitive trace metal concentrations. Fe speciation considers the ratio of Fe_{HR} to total Fe (Fe_T) (Poulton, 2021; Poulton and Canfield, 2005, 2011), and extensive calibration in both modern and ancient (which by definition considers the effects of diagenesis; cf. Pasquier et al., 2022) settings has led to general thresholds to distinguish oxic and anoxic depositional conditions (Raiswell and Canfield, 1998; Raiswell et al., 2001, 2018; Poulton and Raiswell, 2002; Poulton and Canfield, 2011; Clarkson et al., 2014; Poulton, 2021). Oxic water column conditions are commonly indicated when $Fe_{HR}/Fe_T \leq 0.22$, in contrast to ratios ≥ 0.38, which commonly occur due to additional water column precipitation of Fe_{HR} phases under anoxic conditions (Poulton and Canfield, 2005). Intermediate Fe_{HR}/Fe_T ratios (between 0.22 and 0.38) are considered equivocal (Poulton and Canfield, 2011), and additional evidence for water column redox conditions should be considered in these cases. In addition, however, an independent calibration of redox proxy thresholds should be considered for the particular study area where possible (Algeo and Li, 2020; Poulton, 2021), and thus we utilized this approach to provide an oxic Fe_{HR}/Fe_T range for the Welsh Basin (see below).

For anoxic samples, the ratio Fe_{py}/Fe_{HR} can then be used to distinguish between euxinic and ferruginous settings, whereby ratios above 0.6–0.8 commonly indicate euxinia (Anderson and Raiswell, 2004; März et al., 2008; Benkovitz et al., 2020) and ratios ≤ 0.6 imply ferruginous conditions (Poulton and Canfield, 2011; Poulton, 2021). For Fe_{py}/Fe_{HR} ratios, it is not possible to utilize oxic samples to provide a basin-specific calibration of anoxic samples. Hence, to support our interpretation of Fe_{py}/Fe_{HR} ratios based on the calibrated thresholds outlined above, we utilized independent evidence from redox sensitive trace metal systematics.

We also note here recent challenges to the use of Fe speciation as a palaeo-redox proxy (Pasquier et al., 2022). Particular care needs to be taken when Fe speciation is applied to sediments with low Fe

contents (<0.5 wt% Fe_T; Clarkson et al., 2014), sediments resulting from rapid deposition (for example turbidites; Canfield et al., 1996), and those in proximity to hydrothermal inputs (Raiswell et al., 2018) or directly adjacent to (sub)tropical mountainous regions, where highly weathered sediment may supply a high proportion of Fe_{HR} directly onto the continental margin (Wei et al., 2021), thus circumventing the preferential trapping of Fe_{HR} that usually occurs in nearshore environments (Poulton and Raiswell, 2002). However, our calibration of regional oxic baseline values circumvents these potential problems, and our combined approach of using independent redox-sensitive trace metal (specifically U, Mo, Re) systematics provides a particularly robust assessment of the chemical conditions of deposition (Poulton, 2021).

Uranium and molybdenum are highly soluble and exhibit limited enrichment in oxic sediments (Morford et al., 2009). Uranium predominantly exists as U(VI) in uranyl carbonate complexes ($UO_2(CO_3)_3^{4-}$) in oxic seawater (Calvert and Pedersen, 1993), whilst Mo is stable as Mo(VI) in the molybdate oxyanion (MoO_4^{2-}) under such conditions (Zheng et al., 2000). When anoxia develops around the sediment–water interface, soluble U(VI) is reduced to insoluble U(IV), primarily at the onset of the Fe(II)–Fe(III) redox boundary (Anderson et al., 1989). By contrast, the removal of Mo requires the specific presence of relatively high concentrations of HS^- in the water column, resulting in the formation of thiomolybdates ($MoO_xS_4^{x-}$) under euxinic conditions (Helz et al., 1996; Zheng et al., 2002). Finally, Re is enriched in sediments located just below the sediment–water interface (~1 cm) even under weakly reducing (dysoxic) conditions that lack U and Mo enrichment (Crusius et al., 1996).

Thus, combined consideration of Re, U and Mo systematics, alongside Fe speciation, may allow dysoxic, anoxic non-sulfidic (ferruginous) and euxinic conditions to be distinguished. However, oxic baseline values for redox-sensitive trace metals are particularly basin-specific (Algeo and Li, 2020), since there is a strong dependence on the composition of the sediment supplied to the basin. Therefore,

as with Fe_{HR}/Fe_T ratios, we utilize oxic samples from the basin to calibrate baseline depositional values for Re, U and Mo, thus allowing redox-driven enrichments to be fully assessed.

Results

In the Borth and Banwy River sections TOC ranges from 0.11 to 0.28 wt%, with an average of 0.18 ± 0.03 wt% (Fig. 4). In the Buttington section, TOC values are generally higher, ranging from 0.19 wt% to 0.68 wt%, with an average of 0.39 ± 0.03 wt% (Figs. 4 and 5A). Although the data show scatter, there are distinct zones that generally have higher TOC concentrations (up to 0.6–0.7 wt%; Fig. 5A).

The phase partitioning of Fe is relatively constant in the Buttington section (Fig. 5D) and is dominated by reduced Fe phases (i.e., Fe_{carb}, Fe_{mag} and Fe_{py}), with oxidized phases (i.e., Fe_{ox}) accounting for only 7.6 ± 4.2% of the total Fe_{HR} pool. Fe_{HR}/Fe_T ratios average 0.40 ± 0.08 and Fe_{py}/Fe_{HR} ratios average 0.40 ± 0.11 (Fig. 4), with both ratios showing little systematic variation up-section (Fig. 5). By contrast, Fe_{HR}/Fe_T ratios are consistently lower in the Banwy River (average 0.08 ± 0.03) and Borth sections (average 0.08 ± 0.02), whilst Fe_{py}/Fe_{HR} ratios are also very low (Banwy River = 0.03 ± 0.02; Borth = 0.08 ± 0.14; Fig. 4).

Average U/Al and Mo/Al ratios for all three sections fall below average upper continental crust (UCC) compositions (Fig. 4), with the Buttington section having distinctly higher values (U/Al = 0.32 ± 0.04; Mo/Al = 0.13 ± 0.08) than the Banwy River (U/Al = 0.22 ± 0.05; Mo/Al = 0.02 ± 0.01) and Borth (U/Al = 0.22 ± 0.02; Mo/Al = 0.06 ± 0.06) sections (Fig. 4). By contrast, Re/Al ratios are slightly above the UCC value for the Banwy River (0.12 ± 0.03) and Borth (0.10 ± 0.02) sections, but these ratios are again considerably higher in the Buttington section (0.35 ± 0.10; Fig. 4). Through the Buttington section, U/Al ratios are relatively stable (Fig. 5E), whereas Mo/Al ratios show considerable fluctuation, with five clear intervals of higher values (Fig. 5F). Re/Al ratios are relatively stable in the lower part of the section, but show more variability up-section, although there are no consistent trends in the data (Fig. 5G).

Discussion

Establishing an oxic baseline for the Welsh Basin

Whenever possible, redox interpretations should be calibrated for the specific site of interest, since general redox thresholds are often inadequate when applied on a local or regional scale (Algeo and Li, 2020; Poulton, 2021; Takahashi et al., 2021; Li et al., 2023). This is clearly the case in the Welsh Basin, where samples from the Banwy River and Borth sections have Fe_{HR}/Fe_T ratios that fall well below the general oxic baseline value (Poulton and Canfield, 2011), whilst U/Al and Mo/Al ratios are considerably lower than UCC values (Fig. 4). In addition, Re/Al ratios are only slightly elevated in the Banwy River and Borth sections, relative to the UCC values, and the extent of pyritization (i.e., Fe_{py}/Fe_{HR}) is also very low (Fig. 4). These combined geochemical characteristics strongly suggest deposition under oxic bottom water conditions (Tribovillard et al., 2006; Poulton and Canfield, 2011), with the slight enrichment in Re/Al possibly indicating suboxic conditions close to the sediment-water interface. Since there is no evidence for a significant change in the sedimentary provenance on the depositional timescale of these sections (Ball et al., 1992), the Banwy River and Borth sections allow oxic baseline values to be defined (here termed Welsh Basin Oxic (WBO) values; see Fig. 4). For Fe_{HR}/Fe_T ratios, the WBO oxic baseline was determined as the range measured for the Borth and Banwy River sections, whilst for redox sensitive trace metals, the oxic baseline was determined as the average values for the Borth and Banwy River sections ($\pm 1\sigma$).

Redox dynamics on the mid-shelf

The enrichments in Re (relative to the WBO values) that are apparent throughout the Buttington section (Fig. 5G) suggest that the sediment-water interface was at least dysoxic. In addition, however, the highly elevated Fe_{HR}/Fe_T and U/Al ratios (Fig. 5) suggest that bottom water conditions were, at least periodically, fully anoxic. This consistent behaviour between independent redox proxies provides support for robust palaeoredox interpretations. However, the Buttington section is also

characterized by varying degrees of bioturbation (see Fig. 6 and discussion below), suggesting that the bottom waters likely fluctuated between fully anoxic and (at least partially) oxic on short timescales. Bioturbation impacts the geochemical record of sediments affected by fluctuating redox conditions by homogenizing anoxic enrichments in Fe_{HR} and redox sensitive trace metals over the depth interval affected by burrowing (Sperling et al., 2016; Poulton, 2021). Thus, persistent enrichments in both Fe_{HR} and U in sediments that have experienced bioturbation point to repetitive fluctuations between oxic/dysoxic and anoxic bottom water conditions (Poulton, 2021).

In the Buttington section, Fe_{py}/Fe_{HR} ratios below the lower threshold (0.6) for recognition of euxinia (Fig. 5C) suggest dominantly ferruginous conditions when the water column was anoxic. However, care should be taken with this interpretation in bioturbated sediments, since introduction of oxygen into sediment porewaters by the action of bioturbation would re-oxidize sulfide phases, likely resulting in decreased Fe_{py}/Fe_{HR} ratios. In this context, Mo/Al ratios can be used as supporting evidence for the redox state of the water column, due to the requirement for relatively high concentrations of free sulfide to convert soluble molybdate to particle reactive thiomolybdate (Helz et al., 1996; Zheng et al., 2002). This tends to produce relatively high sediment enrichments in Mo, but needs to be considered alongside the caveat that Mo enrichments may also occur under ferruginous conditions via a particle shuttle mechanism. In this scenario, Mo may be drawn down via adsorption to Fe (oxyhydr)oxide minerals precipitated in the ferruginous water column, which generally gives moderate sediment enrichments (e.g., Algeo and Tribovillard, 2009; Tribovillard et al., 2012).

Our data show several repetitive intervals of increased enrichments in Mo (Fig. 5F), despite the potential for subsequent remobilization and loss of Mo from the sediment during short-lived oxic interludes when intense bioturbation occurred (see below). To resolve whether these enrichments reflect drawdown under dominantly euxinic conditions or drawdown via a particulate shuttle mechanism under dominantly ferruginous conditions, a crossplot of U_{EF} versus Mo_{EF} (where EF

represents the enrichment factor of a particular element) is commonly used (Fig. 7; Algeo and Tribovillard, 2009; Tribovillard et al., 2012). Enrichment factors are normally calculated relative to average continental crust (e.g., UCC), but for our samples, where we have demonstrated that average continental crust does not adequately reflect the composition of the terrestrial sediment delivered to the basin, we instead utilize our average WBO data. Thus, we calculate EFs as $element_{EF}$ = $(element/Al)_{sample}/(element/Al)_{WBO}$.

Figure 7 shows that the data plot on a trajectory indicative of a progressive increase in the intensity of reducing conditions (Algeo and Tribovillard, 2009; Tribovillard et al., 2012). However, the data do not plot in the normal oxic through to euxinic phase space for marine sediments, likely because the impact of bioturbation also needs to be considered. In this context, both U and Mo would be increasingly remobilized from the sediment as bioturbation intensity increases, due to the introduction of oxygenated seawater and reoxidation of a proportion of the U and Mo that was originally sequestered as reduced authigenic phases. Therefore, we also consider the basic trajectories that bioturbation would impart on the broad position of the different redox and particulate shuttle zones (see Figure 7).

Our approach clearly demonstrates that the Buttington data reflect changes in the intensity of reducing conditions (Fig. 7), with intervals where fluctuations between oxic and ferruginous conditions occurred on short timescales (which we term intervals OF1–OF6; Fig. 5). These intervals were, however, separated by periods where the lower water column was likely dominantly euxinic (intervals E1–E5; Fig. 5). As highlighted above, these dominantly euxinic intervals (as identified by Mo enrichments) do not coincide with Fe_{py}/Fe_{HR} enrichments indicative of euxinia (Fig. 5), likely due to partial reoxidation of pyrite during short-lived oxic intervals. Burrowing during these oxic intervals only produced bioturbation indices in the range of 1 – 3 (Fig. 6), although small-scale burrowing by meiofauna could also have contributed without causing visible burrows. However, during bioturbation, anoxic Fe_{HR}/Fe_T enrichments would have been preserved due to the immediate re-

precipitation of pyrite Fe as (oxyhydr)oxide phases. Thus, the combined geochemical signals are entirely consistent with intervals where deposition dominantly occurred under euxinic conditions, but with short-lived periods of better oxygenated conditions promoting limited bioturbation of the sediments (see Fig. 6). This dichotomy between geochemical proxies that record long-term redox conditions, and palaeoecological data that record short-term, better oxygenated interludes, is often encountered in ancient redox studies (e.g. Wignall 1994)

Redox controls on the benthic biota and cause of the IEE

Bioturbation intensity varies considerably at Buttington (Loydell and Large, 2019), with several intervals also being characterized by relatively low biotic diversity (Fig. 6). To investigate the potential roles of anoxia and sulfide toxicity on the biota, we recast the geochemical data in terms of Mo/U and Mo/Re ratios (Fig. 6), whereby high values denote elevated availability of dissolved sulfide in the water column and during early diagenesis. The euxinic intervals E3 and E5, and to a lesser extent E4, correspond with intervals of low bioturbation intensity and very low benthic diversity at times of prolonged euxinia (Fig. 6). By contrast, the first two, shorter-lived euxinic intervals (E1 and E2) show little distinct impact in terms of either bioturbation intensity or benthic diversity. This may be because the ecosystem was placed under progressive strain by each subsequent interval of euxinia, leading to increasingly detrimental consequences for the biota, or alternatively, the timescale of each euxinic pulse may have been critical, with longer intervals having a more pronounced impact. In this latter context, we also note that the sediment deposited during the first two shorter euxinic pulses would mostly have been within the potential bioturbation depth zone when the system recovered from euxinia. Hence, for these shorter euxinic pulses, the bioturbation index and benthic diversity parameters may have been overprinted by subsequent bioturbation when the system recovered to a more amenable oxic-ferruginous state.

In addition, some of the fluctuating oxic-ferruginous intervals (particularly OF2, OF3, OF5 and OF6) are also characterized by relatively low diversity (but not to the extent of the euxinic intervals), although bioturbation intensity appears largely unaffected (Fig. 6). We speculate that variability in the biotic response during these oxic-ferruginous intervals may reflect changes in the relative persistence of oxic vs anoxic conditions, with intervals of relatively prolonged or more frequent oxygenation promoting increased diversity.

Overall, the consistent lithofacies throughout the Buttington section suggests that benthic fauna likely experienced uniform substrate conditions. As a result, variations in bioturbation activity were likely more influenced by changes in redox conditions than substrate consistency, with euxinia exerting a particularly strong impact. Benthic faunas demonstrate distinct evolutionary behaviours in response to varying oxygenation levels (Wignall, 1990). At Buttington, several benthic groups, including trilobites, brachiopods, bivalves and gastropods, were relatively unaffected during the oxic-ferruginous intervals (Fig. 6). By contrast, survival of the benthos was more challenging in the dominantly euxinic intervals (Fig. 6).

Our analysis of the Buttington section reveals dynamic, high amplitude redox changes in this mid-shelf setting during an interval that marks the early stages of the Ireviken extinction crisis, immediately before and during the onset of the Early Sheinwoodian CIE (Fig. 2). The extinction interval was characterized by a graptolite crisis, which persisted until the early *riccartonensis* Zone (Loydell and Large, 2019). The graptolite losses therefore correspond to the highly variable redox conditions at Buttington, but it remains to be seen if these variations are repeated in other regions and locations. It is notable, however, that the earlier major graptolite extinction that occurred during the first phase of the end-Ordovician mass extinction (at the end of the Katian Stage) has also been ascribed to rapid redox variations, rather than persistent anoxia (Kozik et al., 2022). It therefore appears likely that the dynamic fluctuations in marine redox conditions observed at Buttington may

have played a significant role in the biotic crisis during the early Sheinwoodian Stage of the Silurian Period.

A broader scale Oceanic Anoxic Event (OAE) has been proposed for this time interval (Emsbo, 2010), which may have been triggered by a substantial increase in primary production (Young et al., 2019; Cichon-Pupiensis et al., 2021), while an alternative hypothesis involves a marine sedimentary-exhalative brine event (Emsbo, 2017). Our data provide little direct insight into the primary driver(s) of anoxia at this time. However, both the broader scale redox fluctuations between ferruginous and euxinic conditions, and the shorter-term transitions to better oxygenated conditions, likely reflect changes in the position of the chemocline, or a migrating oxygen minimum zone (OMZ), highlighting that at least in mid shelf locations, redox conditions were highly unstable. Indeed, the Mo/Al ratios suggest a degree of cyclicity in the data (particularly if the two shorter euxinic intervals towards the base of the section are considered as one broader interval), and we note that these euxinic intervals commonly occur coincident with the zones that generally have higher TOC concentrations (Fig. 5). This potential cyclicity hints at a possible orbital control on the broader-scale redox fluctuations, but at present this remains speculative and requires further detailed study.

Conclusions

Our independent redox proxy data from two deep-water sections in the Welsh Basin, UK, provide oxic baseline values for this trace-metal-lean region during the early Silurian. These calibrations allow a detailed evaluation of water column redox conditions in a mid-shelf location at Buttington. We identify an oscillating redox state on the mid-shelf in the early Wenlock, with extended intervals that were characterized by oxic-ferruginous conditions, but with regular transitions to a dominantly euxinic state. Benthos, such as trilobites, brachiopods, bivalves and gastropods, were relatively unaffected during oxic-ferruginous intervals, although the relative intensity of oxic versus ferruginous conditions appears to have been important. These faunas were, however, substantially impacted by

the development of euxinia, highlighting the specific role of toxic hydrogen sulfide as a key factor, on top of the detrimental impact of deoxygenation. Graptolites suffered an extinction crisis at this time, which may have been caused by the difficulties of adaptation to conditions of rapid water-column redox variations, although this idea requires investigation of the redox stability in other regions. However, we note that the main end-Ordovician graptolite extinction event also occurred during an interval of dynamic oceanic redox fluctuations (Kozik et al., 2022).

In summary, our data contribute to a growing geochemical database on the evolution of ocean redox conditions during the early Silurian, and suggest that dynamic fluctuations in regional redox conditions occurred in shelf seas. We thus provide new insight into the nature of more widespread anoxia at this time, as well as the ensuing implications for the biotic record during the Ireviken extinction event.

Acknowledgements

This study was funded by a University of Leeds research training grant (YW), and NERC grant NE/T008458/1 (SWP). We thank Anthony Butcher, Bob Loveridge, Thomas Wignall and Bethany Smith for their help with sample collection.

References

Alcott, L.J., Krause, A.J. et al. 2020. Development of Iron Speciation Reference Materials for Palaeoredox Analysis. Geostandards and Geoanalytical Research, 44, 581-591, https://doi.org/10.1111/ggr.12342.

Algeo, T.J. and Li, C. 2020. Redox classification and calibration of redox thresholds in sedimentary systems. Geochimica et Cosmochimica Acta, 287, 8-26, https://doi.org/10.1016/j.gca.2020.01.055.

Algeo, T.J. and Tribovillard, N. 2009. Environmental analysis of paleoceanographic systems based on molybdenum–uranium covariation. Chemical Geology, 268, 211-225, https://doi.org/10.1016/j.chemgeo.2009.09.001.

Anderson, R., LeHuray, A., Fleisher, M. and Murray, J. 1989. Uranium deposition in Saanich Inlet sediments, Vancouver Island. Geochimica et Cosmochimica Acta, 53, 2205-2213. https://doi.org/10.1016/0016-7037(89)90344-X.

Anderson, T.F. 2004. Sources and mechanisms for the enrichment of highly reactive iron in euxinic Black Sea sediments. American Journal of Science, 304, 203-233, https://doi.org/10.2475/ajs.304.3.203.

Baker, M.L. and Baas, J.H. 2020. Mixed sand–mud bedforms produced by transient turbulent flows in the fringe of submarine fans: Indicators of flow transformation. Sedimentology, 67, 2645-2671, https://doi.org/10.1111/sed.12714.

Ball, T.K., Davies, J.R., Waters, R.A. and Zalasiewicz, J.A. 2009. Geochemical discrimination of Silurian mudstones according to depositional process and provenance within the Southern Welsh Basin. Geological Magazine, 129, 567-572, https://doi.org/10.1017/s0016756800021725.

Benkovitz, A., Matthews, A., Teutsch, N., Poulton, S.W., Bar-Matthews, M. and Almogi-Labin, A. 2020. Tracing water column euxinia in Eastern Mediterranean Sapropels S5 and S7. Chemical Geology, 545, 119627. https://doi.org/10.1016/j.chemgeo.2020.119627.

Bickert, T., Pätzold, J., Samtleben, C. and Munnecke, A. 1997. Paleoenvironmental changes in the Silurian indicated by stable isotopes in brachiopod shells from Gotland, Sweden. Geochimica et Cosmochimica Acta, 61, 2717-2730. https://doi.org/10.1016/S0016-7037(97)00136-1.

Calner, M. 2008. Silurian global events – at the tipping point of climate change Mass Extinction. 21-57, https://doi.org/10.1007/978-3-540-75916-4_4.

Calvert, S. and Pedersen, T. 1993. Geochemistry of recent oxic and anoxic marine sediments: implications for the geological record. Marine Geology, 113, 67-88. https://doi.org/10.1016/0025-3227(93)90150-T.

Canfield, D.E., Raiswell, R., Westrich, J.T., Reaves, C.M. and Berner, R.A. 1986. The use of chromium reduction in the analysis of reduced inorganic sulfur in sediments and shales. Chemical Geology, 54, 149-155, https://doi.org/10.1016/0009-2541(86)90078-1.

Canfield, D.E., Lyons, T.W. and Raiswell, R. 1996. A model for iron deposition to euxinic Black Sea sediments. American Journal of Science, 296, 818-834, http://dx.doi.org/10.2475/ajs.296.7.818.

Cave, R. and Dixon, R. 1993. The Ordovician and Silurian of the Welshpool area. In Woodcock, N.H. and Bassett, M.G. (eds). Geological excursions in Powys, central Wales, 51-84.

Cave, R. and Loydell, D.K. 1997. The eastern margin of the Aberystwyth Grits Formation. Geological Journal, 32, 37-44, https://doi.org/10.1002/(sici)1099-1034(199703)32:1.

Cichon-Pupienis, A., Littke, R., Lazauskienė, J., Baniasad, A., Pupienis, D., Radzevičius, S. and Šiliauskas, L. 2021. Geochemical and sedimentary facies study – Implication for driving

mechanisms of organic matter enrichment in the lower Silurian fine-grained mudstones in the Baltic Basin (W Lithuania). International Journal of Coal Geology, 244, https://doi.org/10.1016/j.coal.2021.103815.

Cramer, B.D. and Saltzman, M.R. 2007. Early Silurian paired $\delta^{13}C_{carb}$ and $\delta^{13}C_{org}$ analyses from the Midcontinent of North America: Implications for paleoceanography and paleoclimate. Palaeogeography, Palaeoclimatology, Palaeoecology, 256, 195-203, https://doi.org/10.1016/j.palaeo.2007.02.032.

Cramer, B.D., Kleffner, M.A., Brett, C.E., McLaughlin, P.I., Jeppsson, L., Munnecke, A. and Samtleben, C. 2010. Paleobiogeography, high-resolution stratigraphy, and the future of Paleozoic biostratigraphy: Fine-scale diachroneity of the Wenlock (Silurian) conodont *Kockelella walliseri*. Palaeogeography, Palaeoclimatology, Palaeoecology, 294, 232-241, https://doi.org/10.1016/j.palaeo.2010.01.002.

Cramer, B.D., Condon, D.J. et al. 2012. U-Pb (zircon) age constraints on the timing and duration of Wenlock (Silurian) paleocommunity collapse and recovery during the "Big Crisis". Geological Society of America Bulletin, 124, 1841-1857, https://doi.org/10.1130/b30642.1.

Crusius, J., Calvert, S., Pedersen, T. and Sage, D. 1996. Rhenium and molybdenum enrichments in sediments as indicators of oxic, suboxic and sulfidic conditions of deposition. Earth and Planetary Science Letters, 145, 65-78. https://doi.org/10.1016/S0012-821X(96)00204-X.

Doyle, K.A., Poulton, S.W., Newton, R.J., Podkovyrov, V.N. and Bekker, A. 2018. Shallow water anoxia in the Mesoproterozoic ocean: Evidence from the Bashkir Meganticlinorium, Southern Urals. Precambrian Research, 317, 196-210, https://doi.org/10.1016/j.precamres.2018.09.001.

Hartke, E.R., Cramer, B.D., Calner, M., Melchin, M.J., Barnett, B.A., Oborny, S.C. and Bancroft, A.M. 2021. Decoupling $\delta^{13}C_{carb}$ and $\delta^{13}C_{org}$ at the onset of the Ireviken Carbon Isotope Excursion: $\Delta^{13}C$ and organic carbon burial (f_{org}) during a Silurian oceanic anoxic event. Global and Planetary Change, 196, https://doi.org/10.1016/j.gloplacha.2020.103373.

Emsbo, P. 2017. Sedex brine expulsions to Paleozoic basins may have changed global marine 87Sr/86Sr values, triggered anoxia, and initiated mass extinctions. Ore Geology Reviews, 86, 474-486, https://doi.org/10.1016/j.oregeorev.2017.02.031.

Emsbo, P., McLaughlin, P., Munnecke, A., Breit, G., Koenig, A., Jeppsson, L. and Verplanck, P. 2010. The Ireviken Event: a Silurian OAE. Geol. Soc. Am, 42, 561.

Helz, G., Miller, C., Charnock, J., Mosselmans, J., Pattrick, R., Garner, C. and Vaughan, D. 1996. Mechanism of molybdenum removal from the sea and its concentration in black shales: EXAFS evidence. Geochimica et Cosmochimica Acta, 60, 3631-3642. https://doi.org/10.1016/0016-7037(96)00195-0.

Hints, O., Killinga, M., Männik, P. and Nestor, V. 2006. Frequency patterns of chitinozoans, scolecodonts, and conodonts in the upper Llandovery and lower Wenlock of the Paatsalu core, western Estonia. Proceedings of the Estonian Academy of Sciences, Geology, 55, 128–155, https://doi.org/10.3176/geol.2006.2.04.

Hughes, H.E. and Ray, D.C. 2016. The carbon isotope and sequence stratigraphic record of the Sheinwoodian and lower Homerian stages (Silurian) of the Midland Platform, UK. Palaeogeography, Palaeoclimatology, Palaeoecology, 445, 97-114, https://doi.org/10.1016/j.palaeo.2015.12.022.

James, D.M.D. 2005. Palaeotopography of the northern portion of the Telychian (Silurian) turbidite basin in central Wales. Geological Journal, 40, 593-601, https://doi.org/10.1002/gj.1028.

Jeppsson, L. 1990. An oceanic model for lithological and faunal changes tested on the Silurian record. Journal of the Geological Society, 147, 663-674. https://doi.org/10.1144/gsjgs.147.4.0663.

Jeppsson, L. 1997. The anatomy of the mid-early Silurian Ireviken Event. Paleontological events: stratigraphic, ecological, and evolutionary implications, 451-492.

Jeppsson, L., Landing, E. and Johnson M.E. 1998. Silurian oceanic events: summary of general characteristics. New York State Museum Bulletin, 491, 239-257.

Kaljo, D. and Martma, T. 2006. Application of carbon isotope stratigraphy to dating the Baltic Silurian rocks. GFF, 128, 123-129, https://doi.org/10.1080/11035890601282123.

Kozik, N.P., Young, S.A. et al. 2022. Rapid marine oxygen variability: Driver of the Late Ordovician mass extinction. Sci. Adv., 8, eabn8345, https://doi.org/10.1126/sciadv.abn8345.

Lehnert, O., Männik, P., Joachimski, M.M., Calner, M. and Frýda, J. 2010. Palaeoclimate perturbations before the Sheinwoodian glaciation: A trigger for extinctions during the 'Ireviken Event'. Palaeogeography, Palaeoclimatology, Palaeoecology, 296, 320-331. https://doi.org/10.1016/j.palaeo.2010.01.009.

Li, S., Wignall, P.B., Xiong, Y., Poulton, S.W. 2023. Calibration of redox thresholds in black shale: Insight from a stratified Mississippian basin with warm saline bottom waters. Geological Society of America Bulletin, in press. https://doi.org/10.1130/B36915.1.

Loydell, D.K. and Cave, R. 1993. The Telychian (Upper Llandovery) stratigraphy of Buttington Brick Pit, Wales. Newsletters on Stratigraphy, 29, 91-103, https://doi.org/10.1127/nos/29/1993/91.

Loydell, D.K. and Cave, R. 1996. The Llandovery-Wenlock boundary and related stratigraphy in eastern mid-Wales with special reference to the Banwy River section. Newsletters on Stratigraphy, 34, 39–64, https://doi.org/10.1127/nos/34/1996/39.

Loydell, D.K. and Frýda, J. 2007. Carbon isotope stratigraphy of the upper Telychian and lower Sheinwoodian (Llandovery–Wenlock, Silurian) of the Banwy River section, Wales. Geological Magazine, 144, 1015-1019, https://doi.org/10.1017/s0016756807003895.

Loydell, D.K., Frýda, J., Butcher, A. and Loveridge, R.F. 2014. A new high-resolution δ^{13}Ccarb isotope curve through the lower Wenlock Series of Buttington Quarry, Wales. GFF, 136, 172-174, https://doi.org/10.1080/11035897.2013.865668.

Loydell, D.K. and Large, R.R. 2019. Biotic, geochemical and environmental changes through the early Sheinwoodian (Wenlock, Silurian) carbon isotope excursion (ESCIE), Buttington Quarry, Wales. Palaeogeography, Palaeoclimatology, Palaeoecology, 514, 305-325, https://doi.org/10.1016/j.palaeo.2018.10.028.

März, C., Poulton, S.W., Beckmann, B., Küster, K., Wagner, T. and Kasten, S. 2008. Redox sensitivity of P cycling during marine black shale formation: Dynamics of sulfidic and anoxic, non-sulfidic bottom waters. Geochimica et Cosmochimica Acta, 72, 3703-3717, https://doi.org/10.1016/j.gca.2008.04.025.

McLennan, S.M. 2001. Relationships between the trace element composition of sedimentary rocks and upper continental crust. Geochemistry, Geophysics, Geosystems, 2, 2000GC000109, https://doi.org/10.1029/2000gc000109.

Morford, J.L., Martin, W.R., François, R. and Carney, C.M. 2009. A model for uranium, rhenium, and molybdenum diagenesis in marine sediments based on results from coastal locations. Geochimica et Cosmochimica Acta, 73, 2938-2960, https://doi.org/10.1016/j.gca.2009.02.029.

Munnecke, A., Samtleben, C. and Bickert, T. 2003. The Ireviken Event in the lower Silurian of Gotland, Sweden – relation to similar Palaeozoic and Proterozoic events. Palaeogeography, Palaeoclimatology, Palaeoecology, 195, 99-124, https://doi.org/10.1016/s0031-0182(03)00304-3.

Oborny, S.C., Cramer, B.D., Brett, C.E. and Bancroft, A.M. 2020. Integrated Silurian conodont and carbonate carbon isotope stratigraphy of the east-central Appalachian Basin. Palaeogeography, Palaeoclimatology, Palaeoecology, 554, https://doi.org/10.1016/j.palaeo.2020.109815.

Pasquier, V., Bryant, R.N., Fike, D.A. and Halevy, I. 2021. Strong local, not global, controls on marine pyrite sulfur isotopes. Sci. Adv., 7, https://doi.org/10.1126/sciadv.abb7403.

Pasquier, V., Fike, D.A., Révillon, S. and Halevy, I. 2022. A global reassessment of the controls on iron speciation in modern sediments and sedimentary rocks: A dominant role for diagenesis. Geochimica et Cosmochimica Acta, 335, 211-230, https://doi.org/10.1016/j.gca.2022.08.037.

Poulton, S.W., 2021, The Iron Speciation Paleoredox Proxy. In Elements in Geochemical Tracers in Earth System Science, Cambridge University Press. https://doi.org/10.1017/9781108847148.

Poulton, S.W. and Canfield, D.E. 2005. Development of a sequential extraction procedure for iron: implications for iron partitioning in continentally derived particulates. Chemical Geology, 214, 209-221, https://doi.org/10.1016/j.chemgeo.2004.09.003.

Poulton, S.W. and Canfield, D.E. 2011. Ferruginous conditions: A dominant feature of the ocean through Earth's history. Elements, 7, 107-112, https://doi.org/10.2113/gselements.7.2.107.

Poulton, S. and Raiswell, R. 2002. The low-temperature geochemical cycle of iron: from continental fluxes to marine sediment deposition. American Journal of Science, 302, 774-805, https://doi.org/10.2475/ajs.302.9.774

Raiswell, R., Hardisty, D.S. et al. 2018. The iron paleoredox proxies: A guide to the pitfalls, problems and proper practice. American Journal of Science, 318, 491-526, https://doi.org/10.2475/05.2018.03.

Richardson, J.A., Lepland, A., Hints, O., Prave, A.R., Gilhooly, W.P., Bradley, A.S. and Fike, D.A. 2021. Effects of early marine diagenesis and site-specific depositional controls on carbonate-associated sulfate: Insights from paired S and O isotopic analyses. Chemical Geology, 584, https://doi.org/10.1016/j.chemgeo.2021.120525.

Rose, C.V., Fischer, W.W., Finnegan, S. and Fike, D.A. 2019. Records of carbon and sulfur cycling during the Silurian Ireviken Event in Gotland, Sweden. Geochimica et Cosmochimica Acta, 246, 299-316, https://doi.org/10.1016/j.gca.2018.11.030.

Saltzman, M.R. 2001. Silurian $\delta^{13}C$ stratigraphy: A view from North America. Geology, 29, https://doi.org/10.1130/0091-7613(2001)029<0671:Scsavf>2.0.Co;2.

Scotese, C. 2014. Atlas of Silurian and Middle-Late Ordovician Paleogeographic Maps (Mollweide Projection). The Early Paleozoic, PALEOMAP Atlas for ArcGIS. Evanston (IL): PALEOMAP Project, 5, 73-80.

Sperling, E. A., Carbone, C., Strauss, J. V., Johnston, D. T., Narbonne, G. M., and Macdonald, F. A. 2016. Oxygen, facies, and secular controls on the appearance of Cryogenian and Ediacaran body and trace fossils in the Mackenzie Mountains of northwestern Canada. Geological Society of America, Bulletin, 128, 558–575. https://doi.org/10.1130/B31329.1.

Stone, P. 2014. The Southern Uplands Terrane in Scotland – a notional controversy revisited. Scottish Journal of Geology 50, 97-123. https://doi.org/10.1144/sjg2014-00.

Takahashi, S., Hori, R.S. et al. 2021. Progressive development of ocean anoxia in the end-Permian pelagic Panthalassa. Global and Planetary Change, 207. https://doi.org/10.1016/j.gloplacha.2021.103650.

Tribovillard, N., Algeo, T.J., Baudin, F. and Riboulleau, A. 2012. Analysis of marine environmental conditions based on molybdenum–uranium covariation – Applications to Mesozoic

paleoceanography. Chemical Geology, 324-325, 46-58, https://doi.org/10.1016/j.chemgeo.2011.09.009.

Tribovillard, N., Algeo, T.J., Lyons, T. and Riboulleau, A. 2006. Trace metals as paleoredox and paleoproductivity proxies: An update. Chemical Geology, 232, 12-32, https://doi.org/10.1016/j.chemgeo.2006.02.012

Trotter, J.A., Williams, I.S., Barnes, C.R., Männik, P. and Simpson, A. 2016. New conodont $\delta^{18}O$ records of Silurian climate change: Implications for environmental and biological events. Palaeogeography, Palaeoclimatology, Palaeoecology, 443, 34-48, https://doi.org/10.1016/j.palaeo.2015.11.011.

Wei, G.-Y., Chen, T. et al. 2021. A chemical weathering control on the delivery of particulate iron to the continental shelf. Geochimica et Cosmochimica Acta, 308, 204-216, https://doi.org/10.1016/j.gca.2021.05.058.

Wignall, P.B. 1990. Observations on the evolution and classification of dysaerobic communities. The Paleontological Society Special Publications, 5, 99-111.

Wignall, P.B. 1994. Black shales. Oxford Monographs on Geology and Geophysics 30, Oxford University Press, 127 pp.

Yan, G., Lehnert, O. et al. 2022. The record of early Silurian climate changes from South China and Baltica based on integrated conodont biostratigraphy and isotope chemostratigraphy. Palaeogeography, Palaeoclimatology, Palaeoecology, 606, https://doi.org/10.1016/j.palaeo.2022.111245.

Young, S.A., Kleinberg, A. and Owens, J.D. 2019. Geochemical evidence for expansion of marine euxinia during an early Silurian (Llandovery–Wenlock boundary) mass extinction. Earth and Planetary Science Letters, 513, 187-196, https://doi.org/10.1016/j.epsl.2019.02.023.

Young, S.A., Benayoun, E., Kozik, N.P., Hints, O., Martma, T., Bergström, S.M. and Owens, J.D. 2020. Marine redox variability from Baltica during extinction events in the latest Ordovician–early Silurian. Palaeogeography, Palaeoclimatology, Palaeoecology, 554, https://doi.org/10.1016/j.palaeo.2020.109792.

Zheng, Y., Anderson, R.F., Van Geen, A. and Kuwabara, J. 2000. Authigenic molybdenum formation in marine sediments: a link to pore water sulfide in the Santa Barbara Basin. Geochimica et Cosmochimica Acta, 64, 4165-4178. https://doi.org/10.1016/S0016-7037(00)00495-6.

Zheng, Y., Anderson, R.F., van Geen, A. and Fleisher, M.Q. 2002. Preservation of particulate non-lithogenic uranium in marine sediments. Geochimica et Cosmochimica Acta, 66, 3085-3092. https://doi.org/10.1016/S0016-7037(01)00632-9.

Figure Captions

Figure 1. A. Global palaeogeography of Laurentia and Baltica in the late Llandovery, Silurian, with the red box showing the location of the Welsh Basin (modified from Scotese, 2014). B. Palaeogeography of the Welsh basin during the *riccartonensis* Biozone (mid-Sheinwoodian) (modified from Loydell and Cave, 1996). C. Stratigraphic correlation between the study sections (after Loydell and Cave, 1996). The red lines represent the sampled zones and the green line represents the duration of the IEE, with the dashes representing uncertainty in the precise timing of the onset.

Figure 2. Correlation of carbon isotope curves at the Buttington and River Banwy sections. Isotope ($\delta^{13}C_{org}$ and $\delta^{13}C_{carb}$) data for the Banwy River section are from Loydell and Frýda (2007) and Cramer et al. (2010), and $\delta^{13}C_{carb}$ data for the Buttington section are from Loydell et al. (2014). IEE = Ireviken Extinction Event, ESCIE = Early Sheinwoodian Carbon Isotope Excursion.

Figure 3. Detailed lithological log of the Buttington section. Modified from Cave and Dixon (1993) and Loydell and Large (2019). GSH = graptolitic shale horizons.

Figure 4. Total organic C, redox proxy data and oxic baseline establishment for the early Silurian Welsh basin. Boxes represent the interquartile range and whiskers represent 1σ. The WBO lines represent the Welsh basin oxic values or ranges for the early Silurian. Specifically, shading on the Fe_{HR}/Fe_T plot represents the WBO oxic baseline range for the Borth and Banwy River sections, and the red dashed lines and shading on the redox sensitive trace metal plots represent the average oxic values and the 1σ range, respectively.

Figure 5. Geochemical data for the Buttington section of the Trewern Brook Mudstone Formation, Wales. Shading on the Fe_{HR}/Fe_T plot represents the WBO oxic baseline range, while dashed lines on the redox-sensitive trace metal plots represent the WBO composition. On the Fe_{HR}/Fe_T plot, published thresholds for general identification of oxic, possibly anoxic and anoxic water column conditions (Poulton and Canfield, 2011) are included for context. However, in this case, these thresholds are superseded by our regional oxic baseline calibration. Dashed lines on the Fe_{py}/Fe_{HR} plot represent calibrated thresholds for the identification of ferruginous, possibly euxinic, and euxinic depositional conditions for anoxic samples (Poulton and Canfield, 2011; Poulton, 2021). Pale blue shading indicates intervals of more reducing conditions (possibly euxinic). *mur.* = *murchisoni*.

Figure 6. Palaeoecological data in the context of TOC concentrations and fluctuations in dissolved sulfide in the water column (indicated by Mo/U and Mo/Re ratios). Bioturbation index and the occurrences of common benthic fossil groups (narrow bar = rare; widest bar = very common) are from Loydell and Large (2019).

Figure 7. Plot of Mo_{EF} vs. U_{EF} for samples from the Welsh basin considered in comparison to modern seawater (Algeo and Tribovillard, 2009; Tribovillard et al., 2012). The impact of bioturbation on the suboxic, anoxic (i.e., ferruginous), euxinic and particulate shuttle zones is shown as dashed lines. The Buttington data are distinguished in terms of the broad intervals identified as being dominantly euxinic (ButtingtonE) and oxic-ferruginous (ButtingtonOF), based on Mo systematics (see Figure 5).

Figure 1.

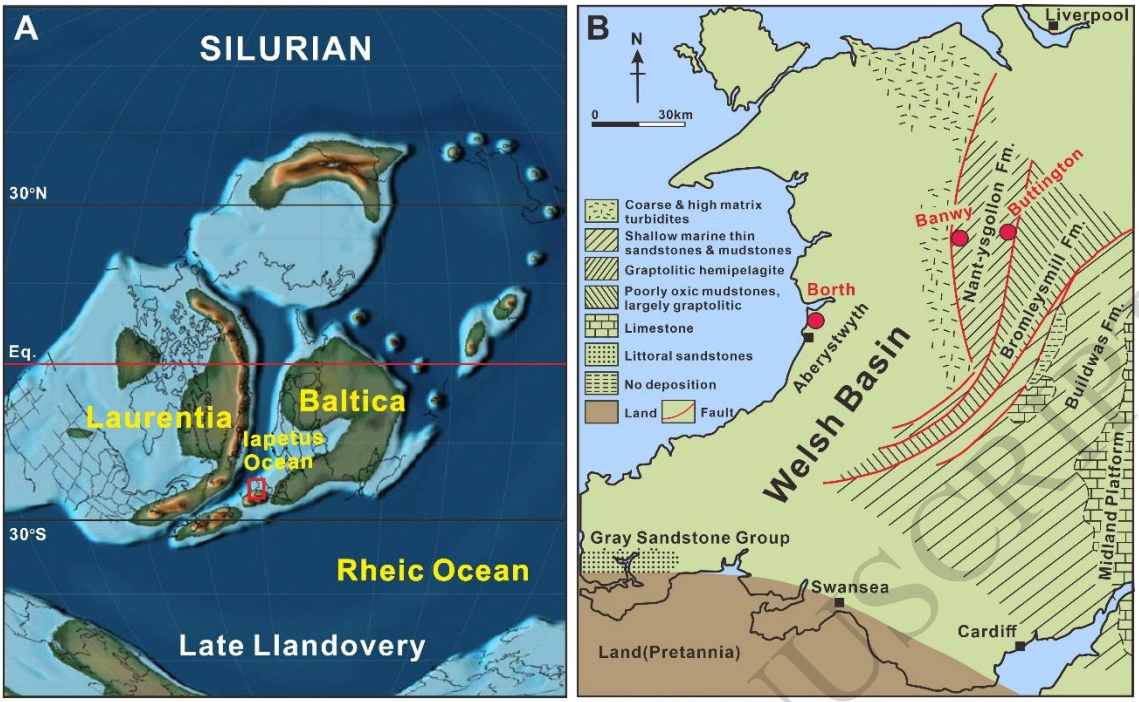

Series	Stage	Biozones	Buttington Section	Banwy River Section	Borth Section
Wenlock	Shein.	*riccartonensis*	Trewern Brook Mudstone Formation	Nant-ysgollon Mudstone Formation	
		firmus			
		murchisoni			
Llandovery	Telychian	*centrifugus*	Butterley Mudstone Member 9m	Banwy Burrowed Member	
		insectus			
		lapworthi			
		spiralis	Tarannon Mudstone Formation 71.2m	Tarannon Mudstone Formation	
		crenulata			
		griestoniensis			
		sartorius			
		crispus			
		turriculatus	Cefn Formation	Laundry Mudstone Formation	Borth Mudstone Formation
		guerichi			

C

Figure 2.

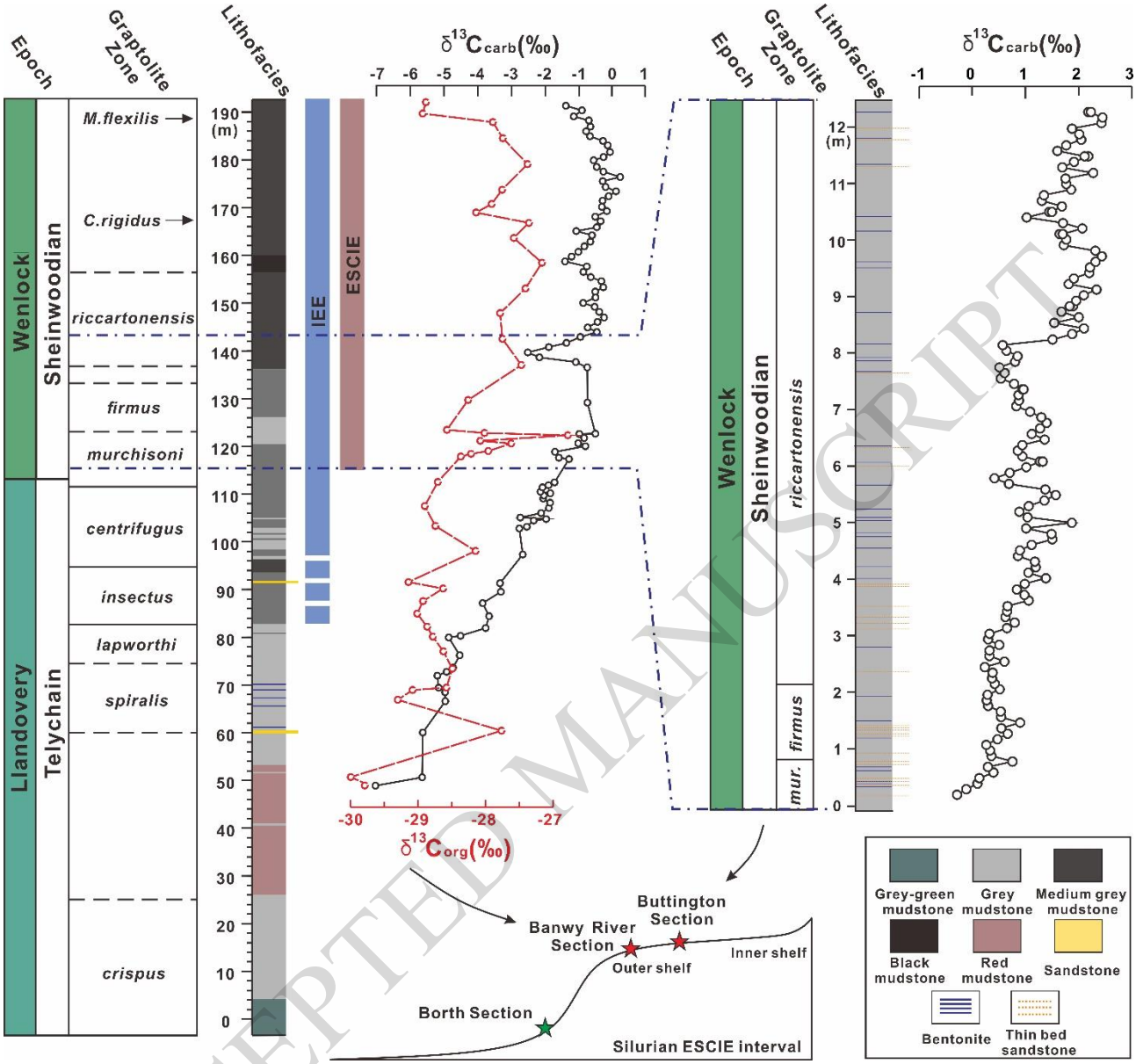

Figure 3.

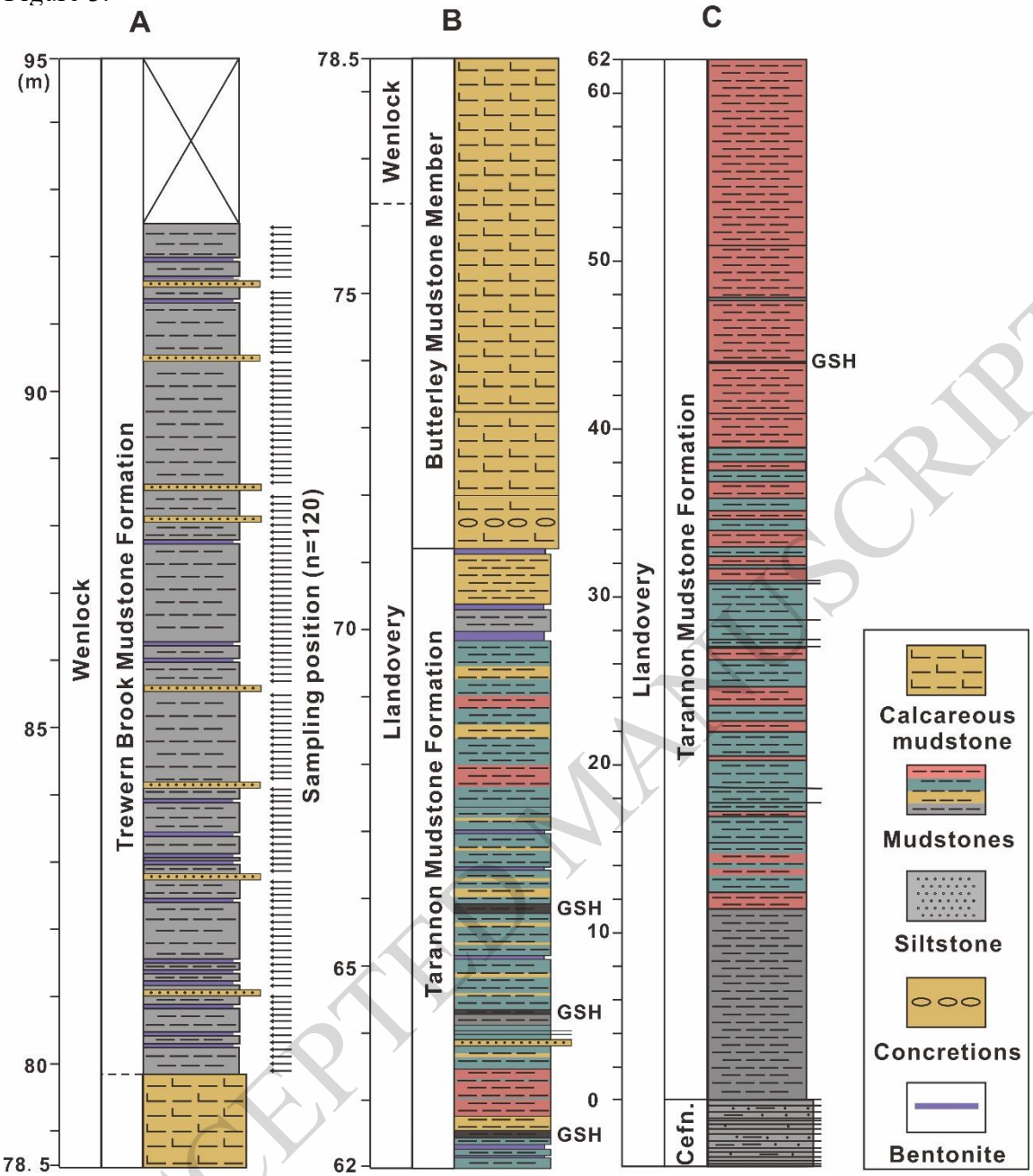

Figure 4.

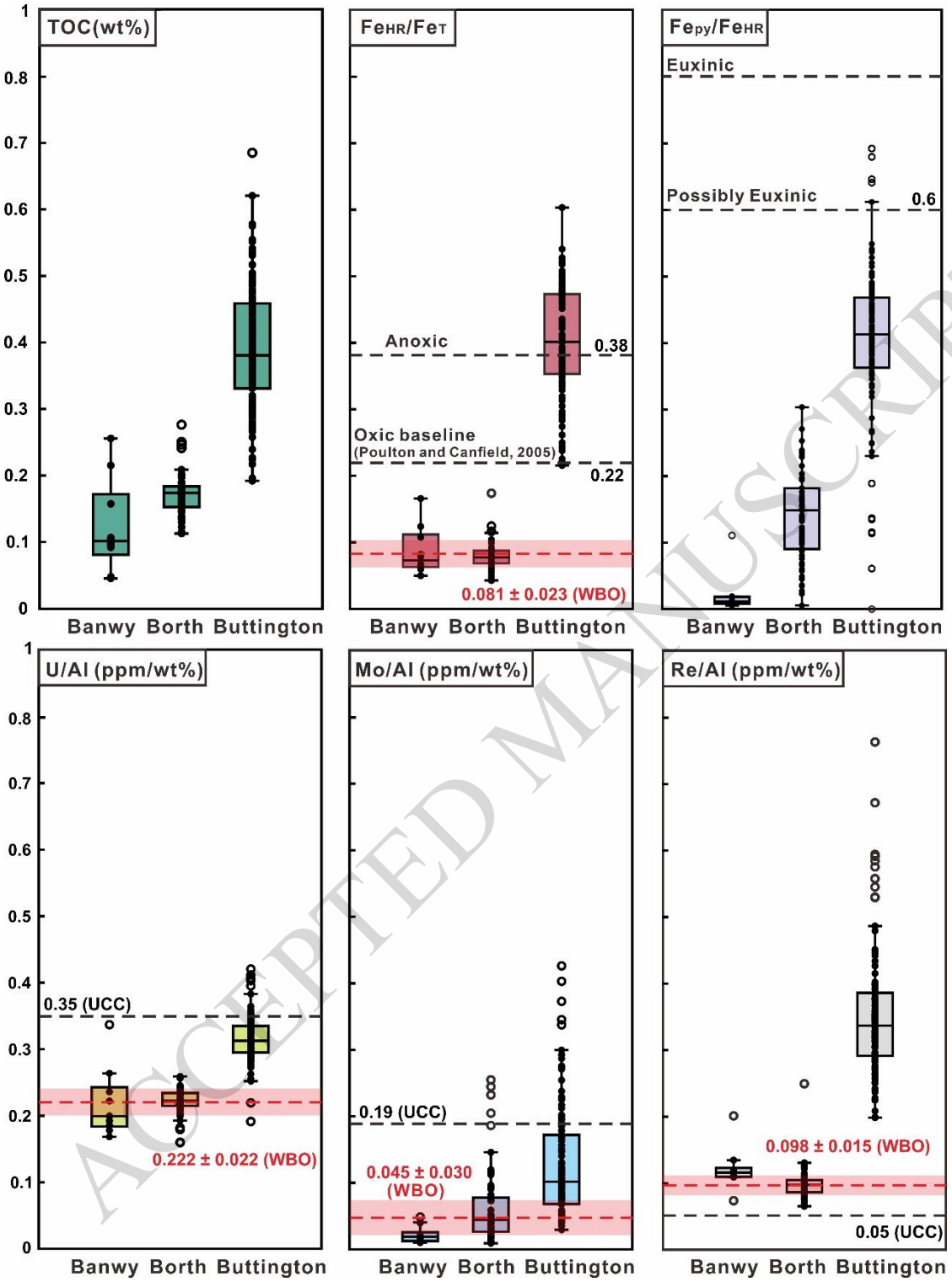

Figure 5.

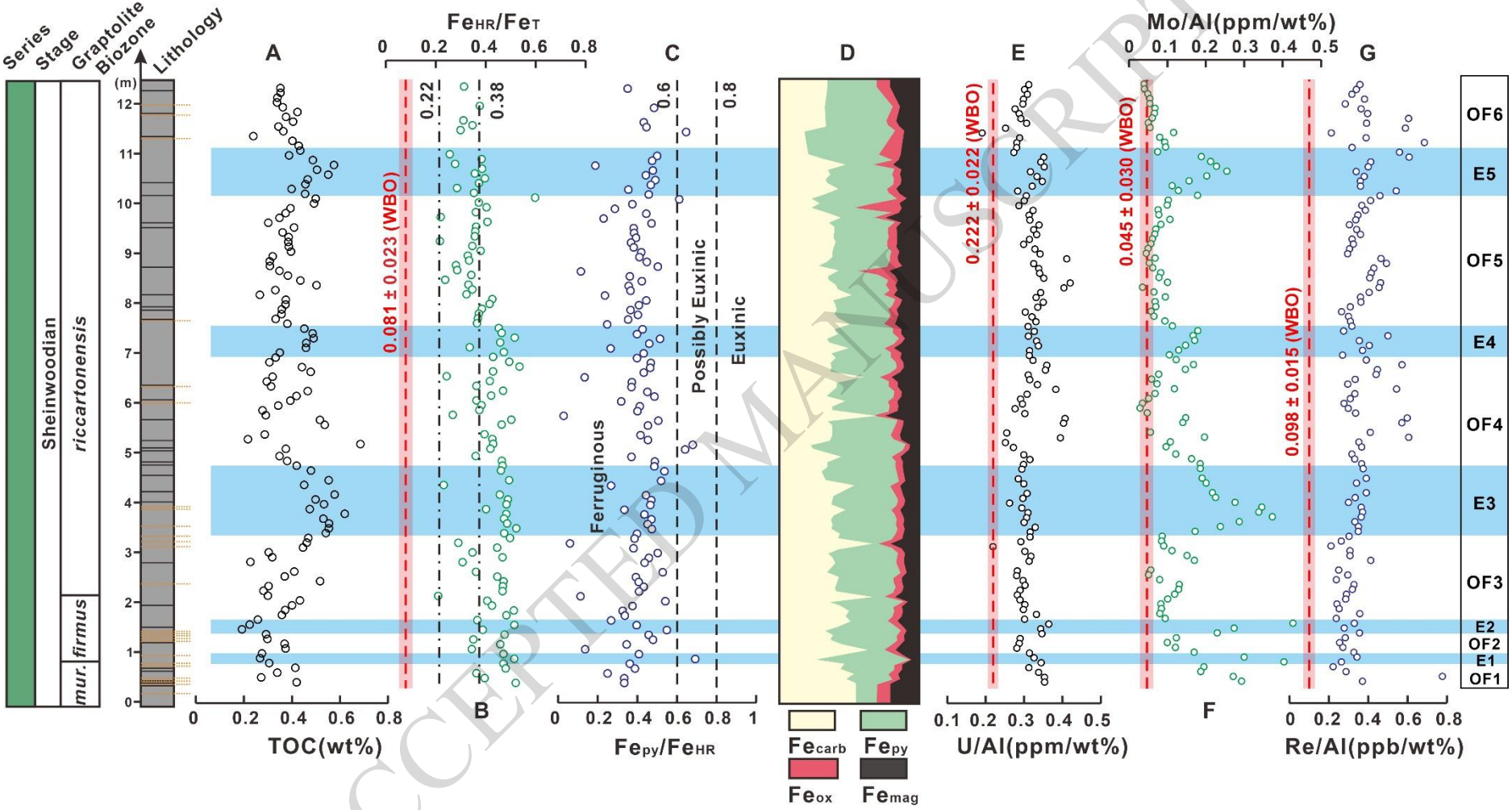

Figure 6.

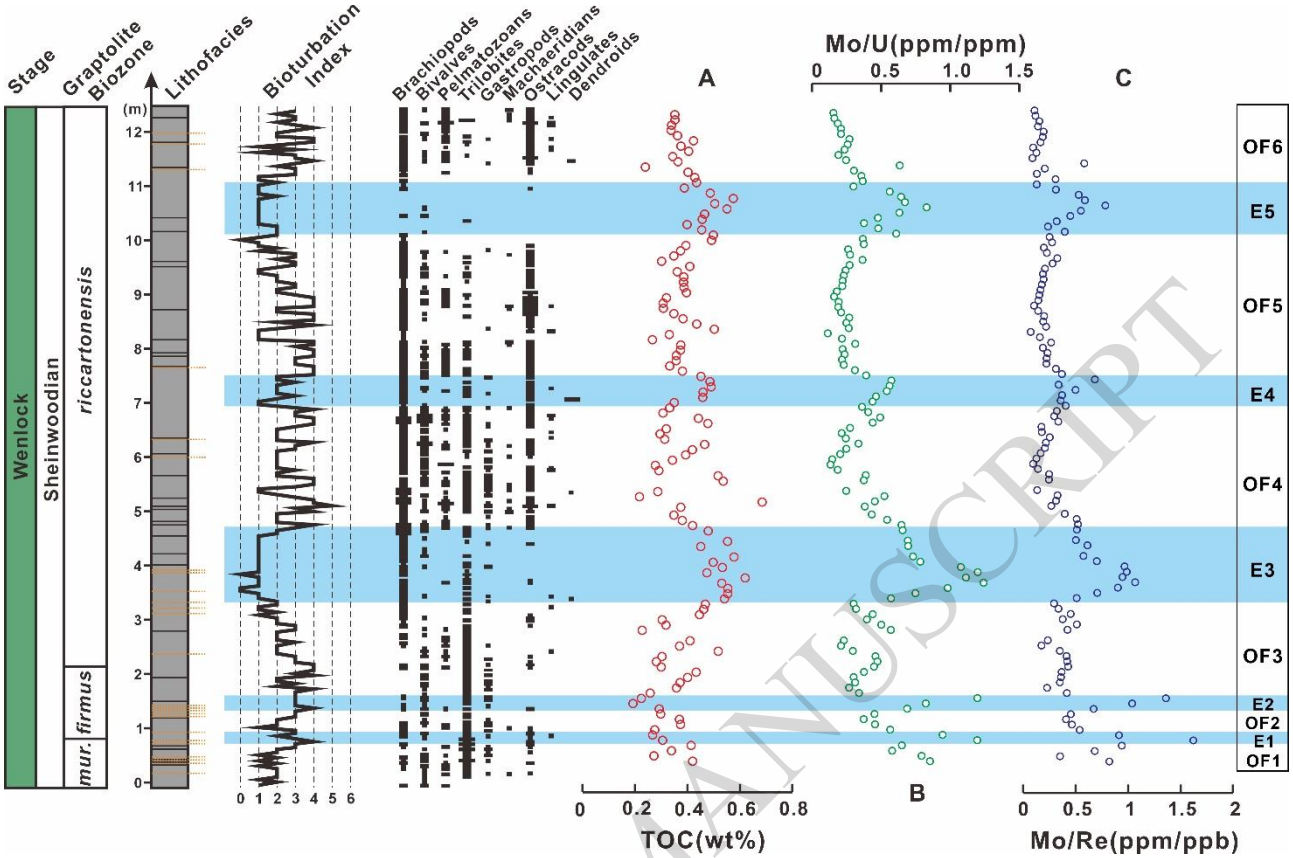

Figure 7.